

Holographic Fermi surfaces in charge density wave from D2-D8

Subir Mukhopadhyay^{*} and Nishal Rai[†]

^{*} Department of Physics, Sikkim University, 6th Mile, Gangtok 737102

[†] Department of Physics, SRM University Sikkim, 5th Mile, Tadong, Gangtok 737102

ABSTRACT

D2-D8 model admits a numerical solution that corresponds to a cdw and an sdw. Considering that as the background, we numerically solve the Dirac equation for probe fermions. From the solution, we obtain the Green's function and study the behaviour of the spectral density. In particular, we have studied the formation of the Fermi surface and where it develops a gap. In addition, we have incorporated an ionic lattice and study its effect on the Fermi surface.

^{*}subirkm@gmail.com.

[†]nishalrai10@gmail.com.

1 Introduction

There are certain strongly correlated electron systems, such as, strange metals in high T_c superconductors and heavy fermion systems [1–3], which admit Fermi surfaces but the excitations are not long-lived and thus live outside the regime of the Fermi liquid theory. Techniques of holography [4–7] have been proved to be quite successful in unravelling various features of such non-Fermi liquids. Especially measurements of Angle Resolved Photoemission Spectroscopy (ARPES) or Scanning Tunneling Microscopy (STM) can be compared with holographic spectral functions leading to a test of holographic applications. Substantial studies of holographic Fermi surfaces have been conducted both in bottom-up [8–15] and top-down [16–29] approaches (see [30] for a review) over the recent past. These works mostly deal with the homogeneous states respecting translational invariance, while on the other hand, there exist real materials, whose ground states are characterised by spontaneously broken translational symmetry and in particular, there are spatially modulated states featured by charge and spin density waves, such as pseudogap regime of cuprate superconductors that break translational symmetry and some or all the symmetries of the underlying lattice [31], which calls for similar studies for such kinds of systems.

Studies of holographic models, simulating the effect of breaking of translational symmetry in homogeneous models appear in a number of works. Gravitational solution with homogeneity are often inflicted with instabilities leading to spatially inhomogeneous solutions as demonstrated in various models in bottom-up [32–49] as well as in top-down approach [50–53]. In particular, [41] considered a bottom-up model with two $U(1)$ gauge fields that leads to a pair density wave with coexistence of a superconducting phase and a charge density wave. Similar inhomogeneous solutions are also obtained for Einstein-Maxwell-dilaton model [43], axionic system [44], higher derivative gravity model with complex scalar and gauge field [47] and a checkerboard solution, which breaks translation symmetry spontaneously in two directions [45]. In the top-down approach, a D3-D7 model has been found to develop instabilities [52] leading to a charge density and a spin density waves [53]. Instabilities of a similar D2-D8 model have been analysed in [50, 51] and found to lead to a combination of spin and charge density waves.

The Fermi surfaces of such spatially modulated solutions obtained from a holographic perspective, have been analysed and several works have appeared on this score. Periodic lattices were introduced by considering perturbatively small periodic modulation of the chemical potential in [54], which was further extended by incorporating the back reaction on the gravity [55]. These lead to anisotropic Fermi surface as well as a band gap at the boundary of the Brillouin zone, though the lattice periodicity is introduced manually and is irrelevant in the infrared. Fermi surfaces have been studied for striped solution obtained in a bottom-up approach with co-existing charge density wave and superconducting phases [56]. In addition, they introduced a lattice by periodic modulation of the chemical potential and studied the Fermi surface. They find when the Fermi surface is

large enough and cross the Brillouin zone boundary, it develops a gap, which increases as the strength of the lattice increases.

The aim of the present work is to study the Fermi surface of the spatially modulated solution obtained in a top-down approach in a D2-D8 model. As mentioned above, instability in a D2-D8 model [50, 51] leads to a combination of charge density and spin density wave, which was obtained numerically in [57]. As has been shown there that this solution is thermodynamically stable with respect to the homogeneous solutions and other instabilities within a domain of the parameter space. We consider the Dirac equation for a generic probe fermion in this background coupled to the gauge field and using holographic techniques study the spectral function of the fermionic operator that couples to the fermion in the gravity theory. In addition to this spontaneous breaking of the translational symmetry, we have also considered effect of an ionic lattice simulated by choosing a periodically varying chemical potential. We find that the dual theory admits Fermi surface once the charge is sufficiently large and as the fermionic charge increases, the Fermi surface crosses the boundary of the Brillouin zone. At the point where two Fermi surfaces intersect, a gap develops. In the presence of an ionic lattice, the gap between the outer and inner parts of the Fermi surface widens. A study of the spectral density function at the inner part indicates that for sufficiently large value of the strength of the ionic lattice, the Fermi surface will reduce to a Fermi arc.

We have organised the paper in the following manner. Section 2 consists of a brief review of the charge and spin density wave solution obtained from the D2-D8 model in [57]. The third section comprises of a discussion of the Dirac equation and the numerical techniques employed. In the fourth section we present the results and we will conclude in the fifth section.

2 D2-D8 model

The model consists of a configuration of a probe D8 brane along with N D2 branes in the background, which due to instability [51, 52] leads to a spatially modulated solution. In [57] a numerical solution ensuing from this instability was obtained, which is characterised by a charge density and a spin density wave and in this section we will review it. If we consider N to be large and the 't Hooft coupling also to be large, $g_s N \gg 1$, this gravity theory is holographically dual to a super Yang-Mills (SYM) theory in $(2+1)$ dimensions. In addition, the dual theory also involves charged fermions that follows from the low energy degrees of freedom of bi-fundamental strings. In addition, we will also introduce effect of an underlying lattice by choosing a chemical potential, which is periodic in the x direction, in which the translational symmetry is explicitly broken.

The ten-dimensional metric and other fields representing the solution associated with

the N D2 branes are given by [51, 52] as follows:

$$\begin{aligned}
ds^2 &= L_0^2[r^{5/2}(-f(r)dt^2 + dx^2 + dy^2) + r^{-5/2}(\frac{dr^2}{f(r)} + r^2 dS_6^2)], \\
dS_6^2 &= d\psi^2 + \sin^2 \psi(d\theta_1^2 + \sin^2 \theta_1 d\phi_1^2) + \cos^2 \psi(d\xi^2 + \sin^2 \xi d\theta_2^2 + \sin^2 \xi \sin^2 \theta_2 d\phi_2^2). \\
f(r) &= 1 - (\frac{r_T}{r})^5, \quad \text{dilaton: } e^\phi = g_s(\frac{r}{L_0})^{-5/4}, \\
\text{five-form potential } C^{(5)} &= c(\psi)L_0^5 d\Sigma_2 \wedge d\Sigma_3
\end{aligned} \tag{2.1}$$

where $d\Sigma_2$ and $d\Sigma_3$ are the volume forms on the S^2 and S^3 respectively, ψ takes values from 0 to $\pi/2$, ξ , θ_1 and θ_2 take values from 0 to π and ϕ_1 , ϕ_2 take values from 0 to 2π . $c(\psi)$ is given by,

$$c(\psi) = \frac{5}{8}(\sin \psi - \frac{1}{6} \sin(3\psi) - \frac{1}{10} \sin 5\psi), \tag{2.2}$$

L_0 is given by $L_0^5 = 6\pi^2 g_s N l_s^5$ and in the following we set $L_0 = 1$.

In this background, there is a probe D8 brane along the directions $t, x, y, r, \theta_1, \phi_1, \xi, \theta_2, \phi_2$. Its position along ψ direction varies over r and x and the function $\psi(r, x)$ represents the embedding. A magnetic field on S^2 given by $2\pi\alpha' F_{\theta_1\phi_1} = L_0^2 b \sin \theta_1$ makes this configuration stable. There is a gauge field a_μ , with $\mu = (t, x, y, r)$, which depends on the radial direction and x and with a choice of a radial gauge one sets $a_r = 0$. One can consider a constant magnetic field h along the xy direction, $2\pi\alpha' F_{xy} = h$ which we choose to be zero for present discussion.

The action is given in the following expression,

$$\begin{aligned}
S &= S_1 + S_2, \\
&= -T_8 \int d^9x e^{-\phi} \sqrt{-\det(g_{\mu\nu} + 2\pi\alpha' F_{\mu\nu})} - \frac{T_8}{2} (2\pi\alpha')^2 \int C^{(5)} \wedge F \wedge F,
\end{aligned} \tag{2.3}$$

where the first term represents DBI action, while the second one is a Chern-Simons term.

For convenience, we trade u for r where $u = \frac{r_T}{r}$. We also scale the worldvolume coordinates $x_\mu = \hat{x}_\mu r_T^{-3/2}$, the gauge field $a_\mu = r_T \hat{a}_\mu$ and the parameter b , $\hat{b} = b\sqrt{r_T}$. In terms of u and the rescaled coordinates, the action reduces to

$$\begin{aligned}
S &= -Nr_T^2 \int du d\hat{x} \frac{1}{u^2} \sqrt{D(D_1 + D_2 + D_3)} - Nr_T^2 \int du d\hat{x} c(\psi)(\hat{a}_{0u}\hat{a}_{\hat{y}\hat{x}} - \hat{a}_{0\hat{x}}\hat{a}_{\hat{y}u}), \\
&= -Nr_T^2 \int du d\hat{x} \frac{1}{u^2} [\sqrt{D(D_1 + D_2 + D_3)} + u^2 c(\psi)(\hat{a}_{0u}\hat{a}_{\hat{y}\hat{x}} - \hat{a}_{0\hat{x}}\hat{a}_{\hat{y}u})],
\end{aligned} \tag{2.4}$$

where in the first and second lines the two terms refer to the DBI action and the Chern-Simons term respectively and $N = 8\pi^3 T_8 V_{1,1}$, $V_{1,1}$ is the volume of spacetime in t and y

direction. D , D_1, D_2 and D_3 are defined as follows:

$$\begin{aligned}
D &= \cos^6 \psi \left(\sin^4 \psi + \frac{\widehat{b}^2}{u} \right), \\
D_1 &= \frac{1}{u^5} [1 + u^2 f \psi_u^2 - u^4 \widehat{a}_{0u}^2 + u^4 f \widehat{a}_{\widehat{y}u}^2 + f u^4 \widehat{a}_{\widehat{x}u}^2] \\
D_2 &= \frac{\psi_{\widehat{x}}^2}{u^2} - \frac{\widehat{a}_{0\widehat{x}}^2}{f} + \widehat{a}_{\widehat{y}\widehat{x}}^2 \\
D_3 &= -u^2 \widehat{a}_{0u}^2 \psi_{\widehat{x}}^2 - u^2 \widehat{a}_{0\widehat{x}}^2 \psi_u^2 + u^2 f \widehat{a}_{\widehat{y}u}^2 \psi_{\widehat{x}}^2 - u^4 \widehat{a}_{0\widehat{x}}^2 \widehat{a}_{\widehat{y}u}^2 + u^2 f \widehat{a}_{\widehat{y}\widehat{x}}^2 \psi_u^2 - u^4 \widehat{a}_{0u}^2 \widehat{a}_{\widehat{y}\widehat{x}}^2 \\
&\quad + 2u^2 \widehat{a}_{0u} \widehat{a}_{0\widehat{x}} \psi_u \psi_{\widehat{x}} + 2u^4 \widehat{a}_{0u} \widehat{a}_{0\widehat{x}} \widehat{a}_{\widehat{y}u} \widehat{a}_{\widehat{y}\widehat{x}} - 2u^2 f \widehat{a}_{\widehat{y}u} \widehat{a}_{\widehat{y}\widehat{x}} \psi_u \psi_{\widehat{x}},
\end{aligned} \tag{2.5}$$

where $\psi_u = \frac{\partial \psi}{\partial u}$, $\widehat{a}_{0\widehat{x}} = \frac{\partial \widehat{a}_0}{\partial \widehat{x}}$, etc. Since $\widehat{a}_{\widehat{x}}$ decouples from the rest of the system we have dropped it.

The equations of motion ensuing from the above action are nonlinear. Nevertheless, these partial differential equations in \widehat{x} and u can be solved using numerical techniques. These equations have the following symmetries: $\widehat{x} \rightarrow -\widehat{x}$, $\widehat{x} \rightarrow \frac{L}{2} - \widehat{x}$ and a reflection symmetry for $h = 0$.

With a chemical potential $\mu(\widehat{x})$, the boundary conditions at the ultraviolet limit, $u = 0$ are,

$$\begin{aligned}
\psi(\widehat{x}, 0) &= \psi_{\infty}, & \partial_u \psi(\widehat{x}, 0) &= m_{\psi}, \\
\widehat{a}_0(\widehat{x}, 0) &= \mu(\widehat{x}), & \widehat{a}_y(x, 0) &= 0,
\end{aligned} \tag{2.6}$$

m_{ψ} represents mass of the fermion, which we have chosen to be non-zero to avoid instabilities arising from tachyons. ψ_{∞} is the asymptotic value of the field ψ at $u \rightarrow 0$, which we have chosen to be constant. In order to simulate the effect of a periodic lattice in the \widehat{x} direction, following [56], we have introduced a periodic variation of the chemical potential

$$\mu(\widehat{x}) = \mu(1 + a_i \cos p\widehat{x}), \tag{2.7}$$

where a_i represents the relative strength of the one-dimensional lattice and p represents the wavevector associated with the lattice. In the present case, we also have an intrinsic wave vector $K = \frac{2\pi}{L}$. In general, they may be different, but once their values are sufficiently close there will be a commensurate lock-in, which may lead to greater stability. In the present discussion we have chosen them to equal.

A periodic boundary condition is imposed along \widehat{x} direction, so that ψ , a_0 and a_y are periodic along \widehat{x} with periodicity L .

At the asymptotic boundary the zeroeth component of the gauge field can be expanded as,

$$a_0(\widehat{x}, u) = \mu(\widehat{x}) + d(\widehat{x})u^2 + \dots, \tag{2.8}$$

where $d(\widehat{x})$ represents the charge density function in the boundary field theory [51, 52].

The average of the charge density over the period is given by

$$\langle d \rangle = \frac{1}{L} \int_0^L d(\hat{x}) d\hat{x}. \quad (2.9)$$

while the amplitude is $\text{Max}(d(\hat{x}) - \langle d \rangle)$.

Similarly, ψ has the following expansion

$$\psi(\hat{x}, u) = \psi_\infty + m_\psi u - c_\psi(\hat{x})u^3 + \dots \quad (2.10)$$

with $c_\psi(\hat{x})$ representing the fermion bilinear in the dual field theory [51, 52]. $\langle c_\psi \rangle$ and $\text{Max}(c_\psi(\hat{x}) - \langle c_\psi \rangle)$ represents the average and the amplitude of the spin density wave in the boundary field theory.

As one may observe, the term $\frac{(\partial_{\hat{x}} \hat{a}_0)^2}{f}$ term in D_2 diverges at the horizon, since f vanishes there. so we set

$$\hat{a}_0(\hat{x}, 1) = 0. \quad (2.11)$$

to have \hat{a} a well-defined one-form at the horizon.

In order to numerically solve the partial differential equations following from the action one can use pseudospectral method [58]. One consider expansion of ψ , a_0 and a_y along u and \hat{x} direction in terms of suitable functions. Along u and \hat{x} one chooses Chebyshev polynomial and Fourier series respectively.

$$\begin{aligned} \psi &= \sum_{m=0}^{N_1-1} \sum_{n=0}^{N_2-1} \psi[m, n] T_m(2u-1) \cos \frac{2\pi n \hat{x}}{L}, \\ \hat{a}_0 &= \sum_{m=0}^{N_1-1} \sum_{n=0}^{N_2-1} a_0[m, n] T_m(2u-1) \cos \frac{2\pi n \hat{x}}{L}, \\ \hat{a}_y &= \sum_{m=0}^{N_1-1} \sum_{n=0}^{N_2-1} a_y[m, n] T_m(2u-1) \sin \frac{2\pi n \hat{x}}{L}. \end{aligned} \quad (2.12)$$

The collocation points along \hat{x} direction are distributed uniformly and the points from $u = 0$ to $u = 1$ form the Gauss-Lobatto grid. The ultraviolet boundary conditions (2.6) reduces the number of the coefficients. Substitution of these expansions in the equations of motion and evaluating them at collocation points leads to a set of algebraic equations, which can be solved using Newton-Rhapson method. The choice in [57] is $N_2 = 9$ and $N_1 = 11$.

The values for the various parameters are determined as follows. As shown in [51, 52], the asymptotic value of ψ at the boundary $u = 0$ should be $\psi_\infty = 0$. If at a finite value of u , $\psi(u)$ vanishes with finite ψ' , self-intersection of D8 brane leads to a conical singularity leading to tachyonic mode, which can be avoided by choosing non-zero m_ψ [51]. In [57], m_ψ and b are chosen as $m_\psi = 0.5$ $b = 1$.

As explained in [57], with this choice of parameters, one can numerically solve the equations and evaluate the free energy for different values of the chemical potential and periodicity. For a given value of the chemical potential, the periodicity corresponds to the minimum of the free energy. Examining the charge density and the spin density these solutions are found to be characterised by charge density wave and spin density wave. There is a domain in the parameter space over which these spatially modulated charge density wave solutions are thermodynamically stable in comparison to a homogeneous solution.

In what follows, we have set the magnetic field h to be zero and the chemical potential μ deep inside the region of stability. The periodicity L follows from the minimum of the free energy. With this solution as the background, we will introduce fermions in the gravity theory and consider the Dirac equation in the following section. Solving the Dirac equation numerically we will obtain the spectral density function and study its behaviour.

3 The Dirac Equation

In order to study the spectral functions associated with the fermionic operators in the dual theory we will begin with the Dirac equation for the fermions in the gravity theory. The Dirac equation is given by

$$[\Gamma^\mu(\nabla_\mu - iqa_\mu) - m]\chi = 0, \quad (3.1)$$

where the gamma matrices are $\Gamma^\mu = e_a^\mu \Gamma^a$, the covariant derivatives are given by $\nabla_\mu \chi = [\partial_\mu + \frac{1}{4}(\omega_\mu)_{ab}\Gamma^{ab}]\chi$, q is the charge of the fermions, a_μ is the background gauge field and m is the mass of the Dirac fermions. We will drop the hats in what follows to avoid the cluttering.

The expressions for the vielbeins e_a^μ follows from the background metric and for our purpose are given by

$$\begin{aligned} e_{\bar{t}} &= \frac{r_T^{1/4} u^{5/4}}{\sqrt{f}} \partial_t, & e_{\bar{x}} &= \frac{r_T^{1/4} u^{5/4}}{\sqrt{1 + u^3 \psi_x^2}} \partial_x, & e_{\bar{y}} &= r_T^{1/4} u^{5/4} \partial_y, \\ e_{\bar{u}} &= r_T^{1/4} u^{3/4} \sqrt{f} \sqrt{\frac{1 + u^3 \psi_x^2}{1 + u^3 \psi_x^2 + u^2 f \psi_u^2}} \left[\partial_u - \frac{u^3 \psi_x \psi_u}{1 + u^3 \psi_x^2} \partial_x \right], \end{aligned} \quad (3.2)$$

where we have used $\bar{t}, \bar{x}, \bar{y}, \bar{u}$ for the tangent space coordinates, $\psi_u = \frac{\partial \psi}{\partial u}$, $\psi_x = \frac{\partial \psi}{\partial x}$.

The gamma matrices are chosen following [54], and are written in terms of the Pauli spin matrices as, $\Gamma^{\bar{t}} = \begin{pmatrix} i\sigma^1 & 0 \\ 0 & i\sigma^1 \end{pmatrix}$, $\Gamma^{\bar{x}} = \begin{pmatrix} -\sigma^2 & 0 \\ 0 & \sigma^2 \end{pmatrix}$, $\Gamma^{\bar{y}} = \begin{pmatrix} 0 & -i\sigma^2 \\ i\sigma^2 & 0 \end{pmatrix}$, $\Gamma^{\bar{u}} = \begin{pmatrix} -\sigma^3 & 0 \\ 0 & -\sigma^3 \end{pmatrix}$.

The spin connection $(\omega_\mu)_{ab}$ can be absorbed by making the following redefinition of the spinors

$$\chi = \frac{r_T^{3/8} u^{5/8}}{(1 + u^3 \psi_x^2)^{1/4}} \begin{pmatrix} \Psi_1 \\ \Psi_2 \end{pmatrix}, \quad (3.3)$$

where $\Psi_\alpha, \alpha = 1, 2$ is a two-component spinor. Since the background is spatially modulated in the x direction with a period fixed by Umklapp wavevector $K = \frac{2\pi}{L}$, the momentum modes that differ by a lattice vector are not independent. In accordance with the Bloch Theorem, we consider the following expansion,

$$\Psi_\alpha = \int \frac{d\omega dk_x dk_y}{2\pi} \sum_{l \in \mathbb{Z}} \mathcal{F}_\alpha^{(l)}(u, \omega, k_x, k_y) e^{-i\omega t + i(k_x + lK)x + ik_y y}, \quad \alpha = 1, 2. \quad (3.4)$$

Here l refers to the different momentum level and k_x is restricted to the first Brillouin zone. We write

$$\mathcal{F}_\alpha(u, x, \omega, k_y) = \sum_{l \in \mathbb{Z}} \mathcal{F}_\alpha^{(l)}(u, \omega, k_x, k_y) e^{ilKx}, \quad (3.5)$$

where \mathcal{F}_α satisfy

$$\mathcal{F}_\alpha(u, x, \omega, k_y) = \mathcal{F}_\alpha(u, x + \frac{2\pi}{K}, \omega, k_y) \quad (3.6)$$

Since Ψ_α is a two component spinor, we further split $\mathcal{F}_\alpha(u, x)$ as

$$\mathcal{F}_\alpha(u, x) = \begin{pmatrix} \mathcal{A}_\alpha(u, x) \\ \mathcal{B}_\alpha(u, x) \end{pmatrix}, \quad \alpha = 1, 2. \quad (3.7)$$

With these splitting, the Dirac equation can be written as,

$$\begin{aligned} & \partial_u \begin{pmatrix} \mathcal{A}_1 \\ \mathcal{B}_1 \end{pmatrix} - \frac{\sqrt{u}}{f} \sqrt{\frac{1 + u^3 \psi_x^2 + u^2 f \psi_u^2}{1 + u^3 \psi_x^2}} (\omega + qa_0) \begin{pmatrix} \mathcal{B}_1 \\ -\mathcal{A}_1 \end{pmatrix} - \frac{u^3 \psi_x \psi_u}{1 + u^3 \psi_x^2} (\partial_x + ik_x) \begin{pmatrix} \mathcal{A}_1 \\ \mathcal{B}_1 \end{pmatrix} \\ & - i \sqrt{\frac{u}{f}} \frac{\sqrt{1 + u^3 \psi_x^2 + u^2 f \psi_u^2}}{1 + u^3 \psi_x^2} (\partial_x + ik_x) \begin{pmatrix} \mathcal{B}_1 \\ \mathcal{A}_1 \end{pmatrix} + \frac{\tilde{m}}{u^{3/4} \sqrt{f}} \sqrt{\frac{1 + u^3 \psi_x^2 + u^2 f \psi_u^2}{1 + u^3 \psi_x^2}} \begin{pmatrix} \mathcal{A}_1 \\ -\mathcal{B}_1 \end{pmatrix} \\ & + i \sqrt{\frac{u}{f}} \sqrt{\frac{1 + u^3 \psi_x^2 + u^2 f \psi_u^2}{1 + u^3 \psi_x^2}} (k_y - qa_y) \begin{pmatrix} \mathcal{B}_2 \\ \mathcal{A}_2 \end{pmatrix} = 0, \\ & \partial_u \begin{pmatrix} \mathcal{A}_2 \\ \mathcal{B}_2 \end{pmatrix} - \frac{\sqrt{u}}{f} \sqrt{\frac{1 + u^3 \psi_x^2 + u^2 f \psi_u^2}{1 + u^3 \psi_x^2}} (\omega + qa_t) \begin{pmatrix} \mathcal{B}_2 \\ -\mathcal{A}_2 \end{pmatrix} - \frac{u^3 \psi_x \psi_u}{1 + u^3 \psi_x^2} (\partial_x + ik_x) \begin{pmatrix} \mathcal{A}_2 \\ \mathcal{B}_2 \end{pmatrix} \\ & + i \sqrt{\frac{u}{f}} \frac{\sqrt{1 + u^3 \psi_x^2 + u^2 f \psi_u^2}}{1 + u^3 \psi_x^2} (\partial_x + ik_x) \begin{pmatrix} \mathcal{B}_2 \\ \mathcal{A}_2 \end{pmatrix} + \frac{\tilde{m}}{u^{3/4} \sqrt{f}} \sqrt{\frac{1 + u^3 \psi_x^2 + u^2 f \psi_u^2}{1 + u^3 \psi_x^2}} \begin{pmatrix} \mathcal{A}_2 \\ -\mathcal{B}_2 \end{pmatrix} \\ & - i \sqrt{\frac{u}{f}} \sqrt{\frac{1 + u^3 \psi_x^2 + u^2 f \psi_u^2}{1 + u^3 \psi_x^2}} (k_y - qa_y) \begin{pmatrix} \mathcal{B}_1 \\ \mathcal{A}_1 \end{pmatrix} = 0. \end{aligned} \quad (3.8)$$

The momentum mode expansion of the different functions \mathcal{A}_α and \mathcal{B}_α are given by

$$\mathcal{A}_\alpha = \sum_{l \in \mathbb{Z}} \mathcal{A}_\alpha^{(l)} e^{ilKx}, \quad \mathcal{B}_\alpha = \sum_{l \in \mathbb{Z}} \mathcal{B}_\alpha^{(l)} e^{ilKx}, \quad (3.9)$$

The boundary condition for solving these first order linear differential equations can be obtained from the near horizon limit $u \rightarrow 1$. After substituting the expressions for the background metric and gauge fields and choosing the near horizon limit one finds that the different momentum modes are satisfying the following conditions in the leading order,

$$\mathcal{A}_\alpha^{(l)} \sim (1-u)^{\pm \frac{i\omega}{5}} a_{\alpha 0}^{(l)}, \quad \mathcal{B}_\alpha^{(l)} \sim (1-u)^{\pm \frac{i\omega}{5}} b_{\alpha 0}^{(l)}. \quad (3.10)$$

We have chosen the minus sign and impose the in-falling boundary conditions [59] as that is the correct choice for holographic computation of retarded Green's function of the dual theory living at the boundary. Furthermore, the equations at the near horizon limit also implies

$$b_{\alpha 0}^{(l)} = -ia_{\alpha 0}^{(l)}. \quad (3.11)$$

In the asymptotic limit near the boundary of the AdS space $u \rightarrow 0$ the Dirac equations (3.8) reduces to up to the leading order,

$$\partial_u \begin{pmatrix} \mathcal{A}_\alpha \\ \mathcal{B}_\alpha \end{pmatrix} + \tilde{m}u^{-3/4} \begin{pmatrix} \mathcal{A}_\alpha \\ -\mathcal{B}_\alpha \end{pmatrix} = 0, \quad (3.12)$$

which implies the asymptotic behaviour of the fermions are given by

$$\mathcal{F}_\alpha = \begin{pmatrix} \mathcal{A}_\alpha \\ \mathcal{B}_\alpha \end{pmatrix} \sim a_\alpha e^{4\tilde{m}u^{1/4}} \begin{pmatrix} 1 \\ 0 \end{pmatrix} + b_\alpha e^{-4\tilde{m}u^{1/4}} \begin{pmatrix} 0 \\ 1 \end{pmatrix}. \quad (3.13)$$

This asymptotic behaviour in terms of the momentum level function becomes

$$\mathcal{F}_\alpha^{(l)} = \begin{pmatrix} \mathcal{A}_\alpha^{(l)} \\ \mathcal{B}_\alpha^{(l)} \end{pmatrix} \sim a_\alpha^{(l)} e^{4\tilde{m}u^{1/4}} \begin{pmatrix} 1 \\ 0 \end{pmatrix} + b_\alpha^{(l)} e^{-4\tilde{m}u^{1/4}} \begin{pmatrix} 0 \\ 1 \end{pmatrix}. \quad (3.14)$$

The retarded Green's function can be obtained from the relation between $a_\alpha^{(l)}$ and $b_\alpha^{(l)}$ as

$$a_\alpha^{(l)}(\omega, k_x, k_y) = \sum_{\alpha', l'} G_{\alpha, l; \alpha', l'}^R(\omega, k_x, k_y) b_{\alpha'}^{(l')}(\omega, k_x, k_y), \quad (3.15)$$

The Green's function is considered in the momentum basis as in the experiments such as ARPES, the photoelectrons are in the definite states of momentum. Following [56] we assume that the dominant response will be in the diagonal momentum channel, though there will be a mixing with other momentum modes. With this assumption the spectral density function can be written as

$$A(\omega, k_x, k_y) = \sum_{l \in \mathbb{Z}} \text{Im}(\text{Tr}(G_{\alpha, l; \alpha', l}^R(\omega, k_x, k_y))), \quad (3.16)$$

where $-\frac{K}{2} \leq k_x \leq \frac{K}{2}$ is chosen to be within the first Brillouin zone and l denotes the momentum level or Brillouin zone.

In order to compute the Green's function, we will follow the method explained in [54]. We denote the boundary conditions to be (α, l) by imposing in-falling boundary condition on the spinor component $\Psi_\alpha^{(l)}$ and setting all other spinor components to be zero. We will write the solution for $a_\alpha^{(l)}$ with (β, k) boundary condition as $a(\alpha, l; \beta, k)$ and in this notation the expression for Green's function (3.15) can be written as

$$a(\alpha, l; \beta, k) = \sum_{\alpha', l'} G^R(\alpha, l; \alpha', l') b(\alpha', l'; \beta, k). \quad (3.17)$$

Writing $a(\alpha, l; \beta, k)$ and $b(\alpha', l'; \beta, k)$ as matrices \mathbf{a} and \mathbf{b} , the relation becomes

$$\mathbf{a} = G^R \cdot \mathbf{b}, \quad G^R = \mathbf{a} \cdot \mathbf{b}^{-1} \quad (3.18)$$

Then the spectral weight follows from the Green's function G^R .

We would like to study the spectral function for the background obtained for D2-D8 intersecting brane system, discussed in the last section. In particular, we are interested in the fermionic response of the charge density and spin density wave background, which was derived in [57]. Since we do not have an analytic solution for that we will employ a numerical procedure to solve the Dirac equations for different in-falling boundary conditions and from that we will get the spectral density function in the next section.

Ideally one should go for the fermions in the gravity theory, that describes the D2-D8 brane system. In the present work, however we will consider the generic fermions in this background as that we will give us more flexibility. In order to keep the analysis simple we will further restrict ourselves, to the case of massless fermions. We will consider the fermions in the probe limit and will not consider the back reaction on the gravity.

4 Results

In this section we will consider the spectral function obtained for various parameters in order to study the Fermi surface. At zero temperature, the Fermi surface appears as a pole of spectral density function. In the present case, we will assume that the Fermi surface will reveal itself through peaks of the spectral density function [27].

Following [27] we assume the plot of the spectral density function vs. momentum at $\omega \rightarrow 0$ will show a peak at around that value of the momentum \mathbf{k}_0 , which corresponds to a Fermi surface. The width of the peak should be of the order of the temperature or less. And finally, at that value of the momentum $\mathbf{k} = \mathbf{k}_0$, plotting spectral density vs. frequency ω will show a peak near $\omega = 0$.

With the above criteria, we study the existence and the features of the Fermi surface in the charge and spin density wave solution that we obtained in the present case of D2-D8 brane. We will begin with the solution in absence of any lattice. Due to spontaneous

breakdown of the translational symmetry the solutions are characterised with a natural length scale associated with the periodicity of the charge density wave. Given a chemical potential, the free energy of the solution varies with the periodicity and the latter is determined by the minimum of the free energy. In the present case, we have chosen the value of the chemical potential to be $\mu = 1.6445$, which is deep inside the region of stability of the charge density wave [57]. The value of the period, at that chemical potential for $a_i = 0$, it turns out to be $L = 0.3725$, implying the Bloch wave vector is given by $K = 16.8676$. So the first Brilluoin zone lies between ± 8.331 . We have also considered non-zero values of the strength of the lattice and keeping the chemical potential same the periodicity turns out to be $L = 0.3155$ for $a_i = 0.2$.

To begin with we consider how the Fermi surface depends on the charges of the fermions. We choose a specific value of k_x to be $k_x = 0$, a small value of the frequency ω to be $\omega = .001$ and plotted the spectral function A vs. k_y for five different values of charges. The plots are given in the Figure.1(a) in absence of the ionic lattice ($a_i = 0$) and in the Figure.1(b) in presence of the ionic lattice ($a_i = 0.2$).

As one can see from the figures, with the increase of the fermionic charge the peaks are getting higher and sharper. This is a general feature of the holographic fermions which holds here as well. With charge q sufficiently less, the peak will become quite shallow and broad indicating absence of the Fermi surface. As the charge increases, position of the peak in k_y moves to the right, in the positive direction. Since $k_x = 0$ it can be associated with the fact that the size of the Fermi circle gets bigger with the increasing charges.

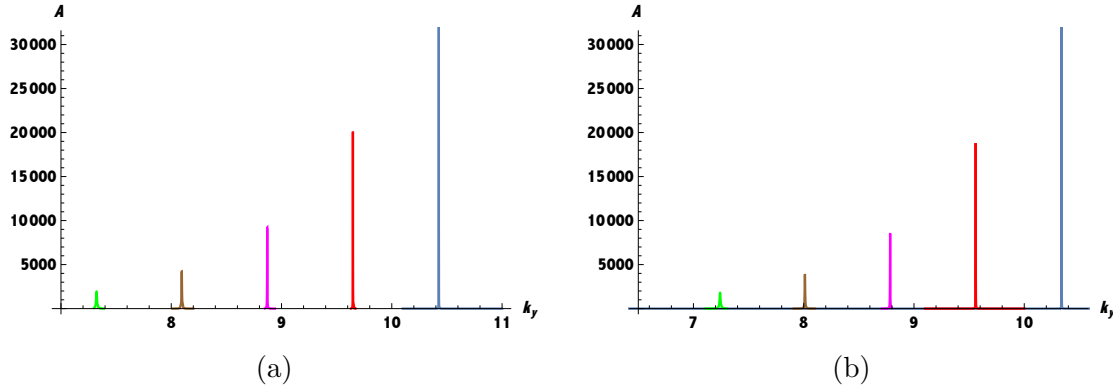


Figure 1: Plot of spectral function A vs. k_y with $k_x = 0$. The peak shifts from right to left with decreasing charges. We have plotted for $q=9$ (blue), 8.5 (red), 8 (magenta), 7.5 (brown), 7 (green). (a) $a_i = 0$ (b) $a_i=0.2$. The height of the plot for $q = 9$ is truncated so as to get all the peaks visible in the figure.

One important topic of interest of the present work is to examine the existence and behaviour of the Fermi surface. We will begin with the model in absence of the ionic lattice. As mentioned earlier, in the present case, we have chosen the value of the chemical potential so as to have the solution deep inside the stability zone. That, in turn determine the periodicity from the minima of the free energy, which determines the size of the

Brillouin zone. For the given periodicity we have chosen the fermionic charge to be $q = 9$ so that the Fermi surface occurs near the boundary of the Brillouin zone. We have given a density plot in the Figure.2, where we have plotted the spectral function vs. k_x and k_y . Since the height of the peaks varies considerably over the region we have given a logarithmic plot of the spectral function. We have numerically computed the values for the first Brillouin zone $-\frac{\pi}{K} \leq k_x \leq \frac{\pi}{K}$ and extended it periodically over k_x .

As one can observe that the Fermi surface consists of intersecting circles with a small eccentricity. At the edge of the Brillouin zone, due to eigenvalue repulsion of degenerate eigenvalues, it opens up a gap in the spectral density. A careful observation would reveal small gaps at the points where the circles intersect as a consequence of the broken translational invariance. The density plot also shows a circle around the origin deep inside the Brillouin zone. With the charge $q = 9$, the height and sharpness of the associated peaks do not qualify to be a Fermi surface. However, with increasing charge it will lead to another Fermi surface. Such nested Fermi surface has been shown in [25].

Since the gaps are not very pronounced in the density plot given in the Figure.2, we have plotted the spectral function vs. k_y at the boundary of the Brillouin zone at $k_x = \frac{\pi}{L}$ in the Figure.3. In order to see the variation of the gap we have computed them for several values of charges as shown in the Figure.3. For higher values of the fermionic charges at the boundary, it shows two adjacent peaks in the value of A with a small valley in between them. As the charge decreases, the heights of the two adjacent peaks decreases and the depth of the intermediate region becoming swallow and thus blurring the gap.

Next we have turned on the ionic lattice and numerically computed the spectral function, which has been given in a density plot in the Figure.4. We have chosen $q = 9$ once again, and set the strength of the ionic lattice to be $a_i = 0.2$. Once again we have obtained intersecting circular Fermi surfaces, which intersects near the boundary of the Brillouin zone. But this time the gaps are wider and It shows small elliptical shapes near the boundary of the Brillouin zone, which we may call inner Fermi surface, separated from the outer boundary of the Fermi surface. The gap increases with increasing strength of the ionic lattice, making the inner Fermi surface smaller. We have further plotted the spectral function A vs. k_x at $k_y = 0$ in the Figure.5 for increasing values of the strength of the ionic lattice from 0 to 0.2. We have chosen $k_y = 0$ as it corresponds to substantial peak associated with the inner Fermi surface. One can observe, the height of the spectral function is decreasing with the increasing strength of ionic lattice. This indicates, for a sufficiently large value of a_i , the strength of the ionic lattice, the inner Fermi surface will disappear leading to a Fermi arc. Such feature has also been found in the context of a bottom-up model, as reported in [60].

In order to study the behaviour of the spectral function with variation of the frequency, we have plotted A vs. ω in the Figure.6. The Figure.6(a) and 6(b) correspond to the plots of spectral function outside and inside the Fermi surface near the boundary. As one can see the peak in A lies at $\omega \geq 0$ and $\omega \leq 0$, respectively, while exactly at the Fermi surface position of the peak coincides with $\omega = 0$, as expected from the criterion of the

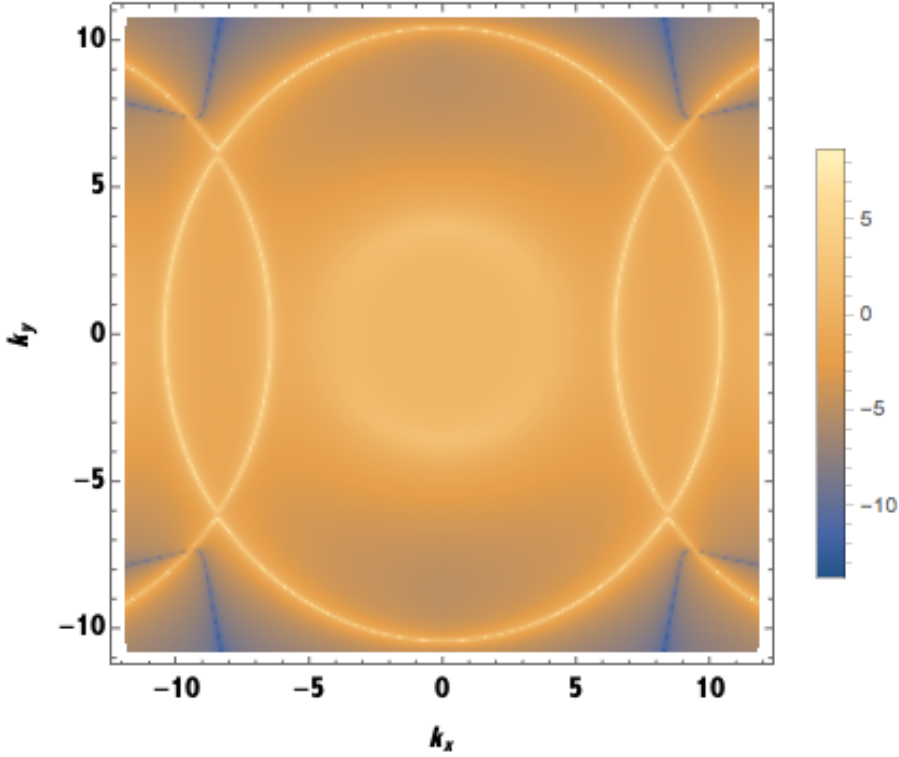


Figure 2: Density Plot of spectral function A over (k_x, k_y) -plane in absence of ionic lattice.

Fermi surface. Figure.6(c) describes the behaviour of the spectral function deep inside the Brillouin zone and far from the Fermi surface. Figure.6(d) is plotted at the boundary of the Brillouin zone on the Fermi surface.

The structure of the plots in all the cases are quite similar qualitatively. It involves two high peaks, whose position depends on the momentum components, (k_x, k_y) . The peak coincides with $\omega = 0$ at the Fermi momentum. These pairs of peaks are accompanied by a valley and a hump like structure on its right hand side. As the Fermi momentum moves away from the Fermi surface, the valley gets flatter and almost vanishes for zero momentum. The gap between the pair of the peaks also varies with the variation of the momentum.

5 Discussion

In this work we have considered fermionic response of a spatially modulated solution obtained in a top-down approach. Intersecting D2-D8 brane system develops instability and for a particular region of the parameter space leads to a solution which consists of a cdw and an sdw. We set the chemical potential to be inside the region of stability and consider that gravitational solution as the background. On top of this solution where translational symmetry is spontaneous broken we have also considered simulating an ionic lattice by introducing periodicity in the chemical potential by hand, which leads to an ex-

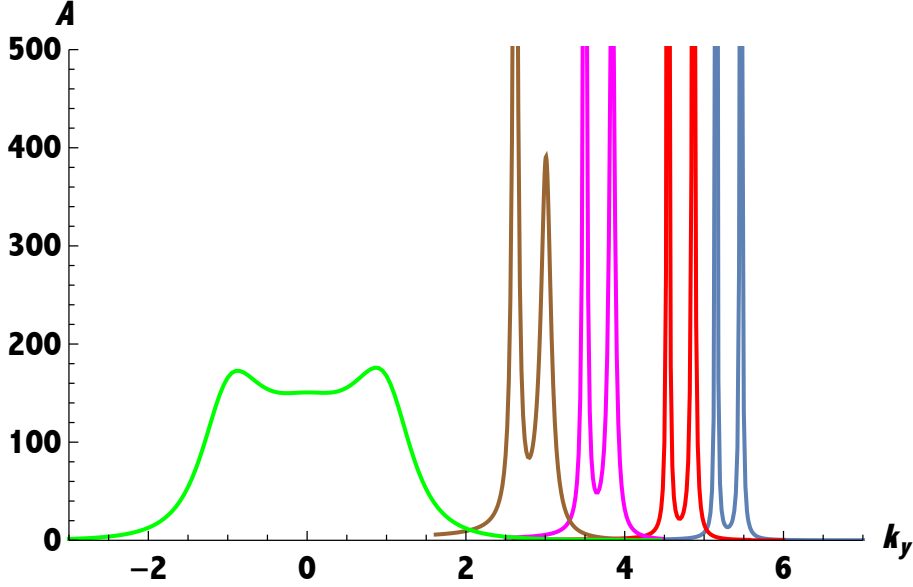


Figure 3: Plot of spectral function A vs. k_y with $k_x = \frac{\pi}{L}$ at the boundary of the Brillouin zone in absence of ionic lattice with different fermionic charges. $q = 8.7$ (blue), 8.5 (red), 8.2 (magenta), 8 (brown), 7.7 (Green). The height of some of the plots are truncated so as to get all the peaks visible in the figure.

explicit breaking of translation symmetry. In this background we introduce generic fermions and numerically solve the Dirac equations. From the asymptotic behaviour of the solutions, we obtain the spectral density associated with the fermionic operators in the dual theory living in the boundary.

In order to study the Fermi surfaces we look for appropriate peak of spectral density function. Due to spontaneous breaking of the translational symmetry, the background solutions are characterised with a periodicity determined by the minimum of the free energy, which in turn depends on the chemical potential. We find as the fermionic charge increases, the height of the peak increases. It shows once the fermionic charge is large enough the Fermi surface materializes. In the present model, plotting the spectral density over momentum plane we obtain the Fermi surface to be a series of circles distributed over the Brillouin zones. As the charge increases further, the circular surfaces get bigger, cross the boundary of the Brillouin zone and intersect. We find at the points of the intersections, they develop a gap and the Fermi surface gets separated into an inner Fermi surface and an outer Fermi surface. In presence of the ionic lattice, the gap becomes more pronounced leading to a wider separation. The height of the spectral density plot is also kept on diminishing with the increasing strength of the ionic lattice. This indicates that for a larger value of the strength of the ionic lattice, the inner Fermi surface will disappear reducing the Fermi surface to Fermi arcs. We have also studied the dependence of the spectral density on the frequency, which are in general characterised by a pair of peaks with a hump like structure separated by a valley-like region.

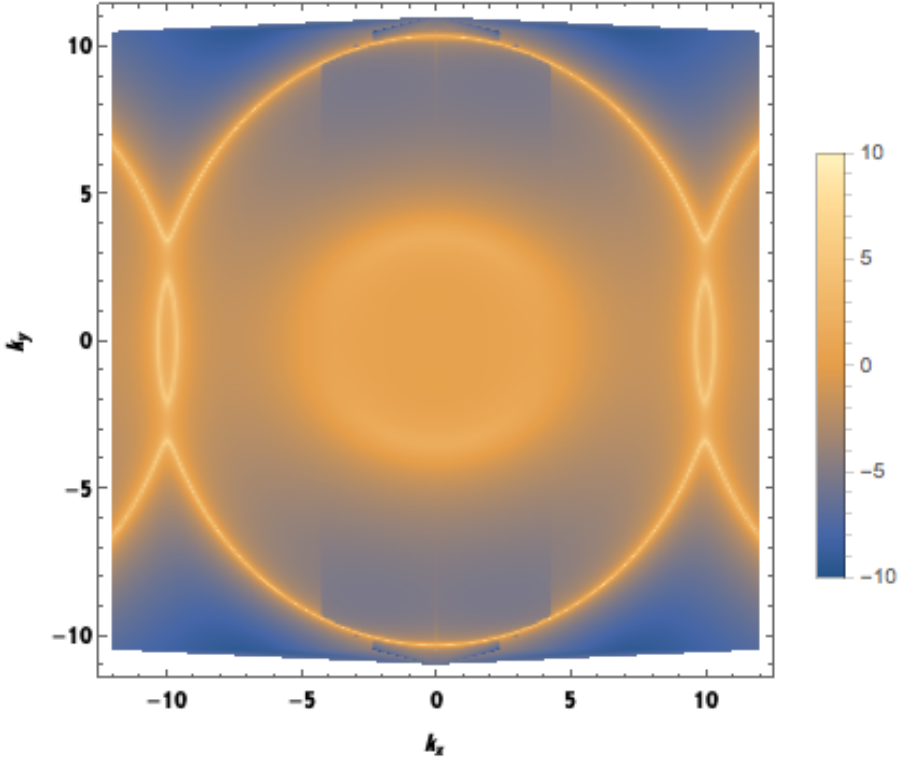


Figure 4: Density Plot of spectral function A over (k_x, k_y) -plane in presence of the ionic lattice with $a_i = 0.2$.

Similar study of Fermi surfaces for a charge density model has appeared in the bottom-up approach [42]. They also obtained similar behaviour of Fermi surfaces suggesting these are generic rather than model dependent features of the charge density wave solutions. In particular, the Fermi arc has been obtained for a larger value of the strength of the ionic lattice in a bottom-up approach [60]. Their study [42] has also reported a peak-dip-hump structure for the plot of the spectral density against the frequency for some region of the momentum space. Such plots in the present model, though similar, show a shallow valley like region rather than a sharp dip.

A natural extension of the present work is to consider the fermionic part of the D2-D8 intersecting brane model and examine the behaviours of the fermions that follows from there. Being a top-down approach it is possible to explicitly consider the exact field theory model dual to it living on the boundary. It will be quite interesting to understand these features in a field theory set-up in the dual model. It will shed light on the formation of the Fermi surfaces and how it reduces to a Fermi arc from the perspective of a field theoretic understanding. The behaviour of the spectral density function with the variation of the frequency also merits a field theoretic study. In fact, a similar study of the spectral functions of the CDW phonons in the case of a CDW superconductor [61] shows quite a similar structure.

We can also extend the analysis for the Majorana fermions. Supergravity models

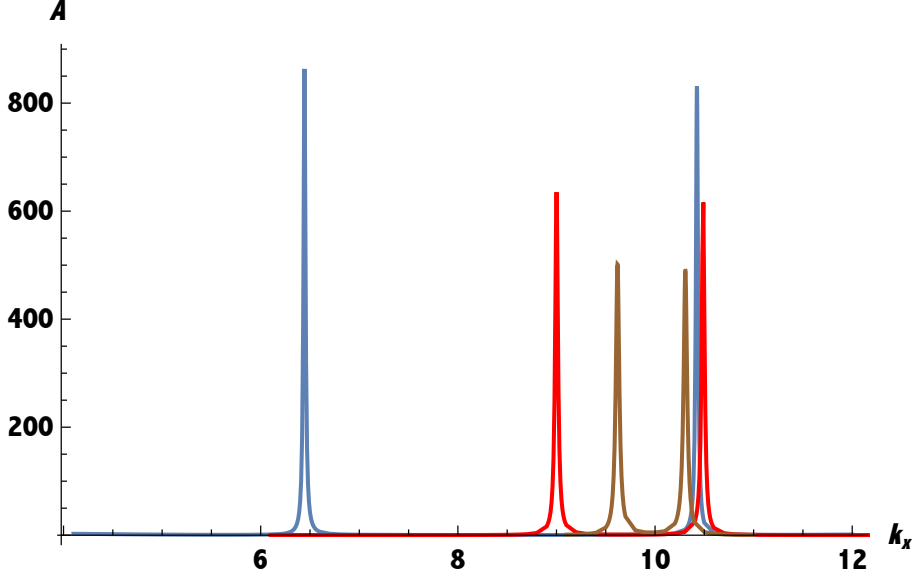


Figure 5: Plot of spectral function A vs. k_x with $k_y = 0$ with different strengths of ionic lattices $a_i = 0$ (blue), 0.1 (red), 0.2 (brown).

often introduce Pauli coupling, which in holographic models introduces gaps in the Fermi surface. It may be interesting to study the implications of the Pauli couplings in the present model and how it modifies the Fermi surface. Lastly, it may be mentioned that the spatially modulated solution that we have considered here is obtained in a probe approximation. One can obtain the full solution by considering the gravitational back reaction, which may provide a more complete picture of the Fermi surface in the present context.

Acknowledgement

SM thankfully acknowledges the financial assistance received from Science and Engineering Research Board (SERB), India (project file no. CRG/2019/002167).

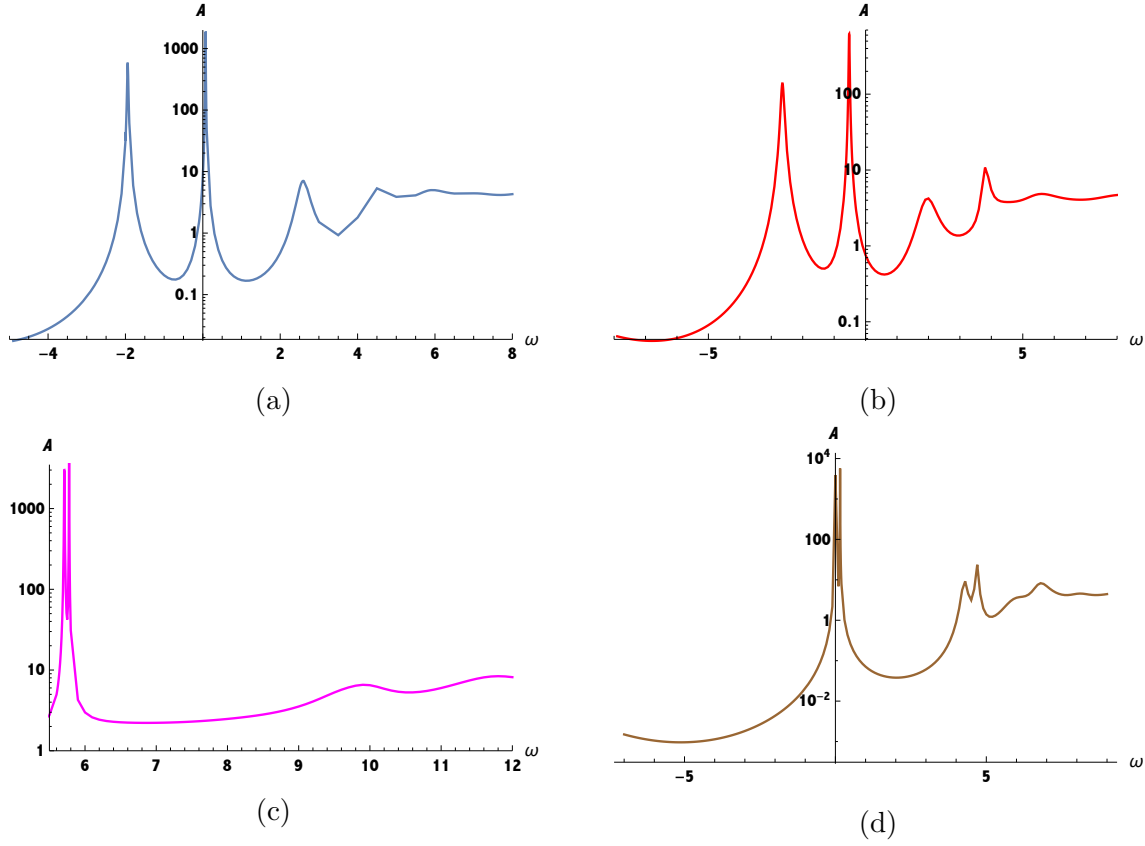


Figure 6: Plot of spectral function A vs. ω with $q = 9$ in absence of ionic lattice; (a) $k_x = 9.8, k_y = 3.8$ (blue), (b) $k_x = 9.8, k_y = 0$ (red), (c) $k_x = 0, k_y = 0$ (magenta), (d) $k_x = 8.43381, k_y = 6.287$ (brown)

References

- [1] C. M. Varma, P. B. Littlewood, S. Schmitt-Rink, E. Abrahams, and A.E. Ruckenstein, “Phenomenology of the normal state of Cu-O high-temperature superconductors,” *Phys. Rev. Lett.* **63**, 1996 (1989).
- [2] “Luttinger-liquid behavior of the normal metallic state of the 2D Hubbard model,” P. W. Anderson, *Phys. Rev. Lett.* **64**, 1839 (1990).
- [3] P. Gegenwart, Q. Si, and F. Steglich, “Quantum criticality in heavy-fermion metals,” *Nat. Phys.* **4**, 186 (2008).
- [4] J. M. Maldacena, “The Large N limit of superconformal field theories and supergravity,” *Int. J. Theor. Phys.* **38**, 1113 (1999), [*Adv. Theor. Math. Phys.* **2**, 231 (1998)], doi:10.1023/A:1026654312961, [hep-th/9711200].

- [5] S. S. Gubser, I. R. Klebanov and A. M. Polyakov, “Gauge theory correlators from noncritical string theory,” *Phys. Lett. B* **428**, 105 (1998), doi:10.1016/S0370-2693(98)00377-3, [hep-th/9802109].
- [6] E. Witten, “Anti-de Sitter space and holography,” *Adv. Theor. Math. Phys.* **2**, 253 (1998), [hep-th/9802150].
- [7] S. A. Hartnoll, Lectures on holographic methods for condensed matter physics, *Class. Quant. Grav.* **26**, 224002 (2009) doi:10.1088/0264-9381/26/22/224002 [arXiv:0903.3246 [hep-th]].
- [8] S. S. Lee, “A Non-Fermi Liquid from a Charged Black Hole: A Critical Fermi Ball,” *Phys. Rev. D* **79**, 086006 (2009), doi:10.1103/PhysRevD.79.086006, [arXiv:0809.3402 [hep-th]].
- [9] M. Henningson and K. Sfetsos, “Spinors and the AdS/CFT correspondence,” *Phys. Lett. B* **431** (1998) 63 [hep-th/9803251].
- [10] W. Mueck and K. S. Viswanathan, “Conformal field theory correlators from classical field theory on antide Sitter space: vector and spinor fields,” *Phys. Rev. D* **58** (1998) 106006 [hep-th/9805145].
- [11] M. Cubrovic, J. Zaanen and K. Schalm, “String Theory, Quantum Phase Transitions and the Emergent Fermi-Liquid,” *Science* **325**, 439 (2009), doi:10.1126/science.1174962 [arXiv:0904.1993 [hep-th]].
- [12] H. Liu, J. McGreevy and D. Vegh, “Non-Fermi liquids from holography,” *Phys. Rev. D* **83**, 065029 (2011) doi:10.1103/PhysRevD.83.065029, [arXiv:0903.2477 [hep-th]].
- [13] T. Faulkner, H. Liu, J. McGreevy and D. Vegh, “Emergent quantum criticality, Fermi surfaces, and AdS(2),” *Phys. Rev. D* **83**, 125002 (2011) doi:10.1103/PhysRevD.83.125002 [arXiv:0907.2694 [hep-th]].
- [14] M. Edalati, R. G. Leigh, K. W. Lo and P. W. Phillips, “Dynamical Gap and Cuprate-like Physics from Holography,” *Phys. Rev. D* **83**, 046012 (2011), doi:10.1103/PhysRevD.83.046012
- [15] M. Edalati, R. G. Leigh and P. W. Phillips, “Dynamically Generated Mott Gap from Holography,” *Phys. Rev. Lett.* **106**, 091602 (2011), doi:10.1103/PhysRevLett.106.091602 [arXiv:1010.3238 [hep-th]].
- [16] M. Ammon, J. Erdmenger, M. Kaminski and A. O’Bannon, “Fermionic Operator Mixing in Holographic p-wave Superfluids,” *JHEP* **1005**, 053 (2010), doi:10.1007/JHEP05(2010)053, [arXiv:1003.1134 [hep-th]].

- [17] K. Jensen, S. Kachru, A. Karch, J. Polchinski and E. Silverstein, “Towards a holographic marginal Fermi liquid,” *Phys. Rev. D* **84**, 126002 (2011), doi:10.1103/PhysRevD.84.126002, [arXiv:1105.1772 [hep-th]].
- [18] J. P. Gauntlett, J. Sonner, and D. Waldram, “Universal Fermionic Spectral Functions from String Theory,” *Phys. Rev. Lett.* **107**, 241601 (2011).
- [19] R. Belliard, S. S. Gubser, and A. Yarom, “Absence of a Fermi surface in classical minimal four-dimensional gauged supergravity,” *J. High Energy Phys.* **10** (2011) 055, doi:10.1007/JHEP10(2011)055, [arXiv:1106.6030]
- [20] J. Gauntlett, J. Sonner, and D. Waldram, “Spectral function of the supersymmetry current,” *J. High Energy Phys.* **11** (2011) 153.
- [21] M. Berkooz, A. Frishman, and A. Zait, “Degenerate rotating black holes, chiral CFTs and Fermi surfaces I Analytic results for quasinormal modes,” *J. High Energy Phys.* **08** (2012) 109.
- [22] M. Berkooz, D. Reichmann, and J. Simon, “A Fermi surface model for large supersymmetric AdS5 black holes,” *J. High Energy Phys.* **01** (2007) 048.
- [23] M. Berkooz and D. Reichmann, “Weakly renormalized near $1/16$ SUSY Fermi liquid operators in Script $N = 4$ SYM,” *J. High Energy Phys.* **10** (2008) 084.
- [24] O. DeWolfe, S. S. Gubser and C. Rosen, “Fermi Surfaces in Maximal Gauged Supergravity,” *Phys. Rev. Lett.* **108**, 251601 (2012), doi:10.1103/PhysRevLett.108.251601 [arXiv:1112.3036 [hep-th]].
- [25] O. DeWolfe, S. S. Gubser and C. Rosen, “Fermi surfaces in $N=4$ Super-Yang-Mills theory,” *Phys. Rev. D* **86**, 106002 (2012), doi:10.1103/PhysRevD.86.106002, [arXiv:1207.3352 [hep-th]].
- [26] O. DeWolfe, O. Henriksson and C. Rosen, “Fermi surface behavior in the ABJM M2-brane theory,” *Phys. Rev. D* **91**, no. 12, 126017 (2015), doi:10.1103/PhysRevD.91.126017, [arXiv:1410.6986 [hep-th]].
- [27] C. Cosnier-Horeau and S. S. Gubser, “Holographic Fermi surfaces at finite temperature in top-down constructions,” *Phys. Rev. D* **91**, no. 6, 066002 (2015), doi:10.1103/PhysRevD.91.066002 [arXiv:1411.5384 [hep-th]].
- [28] S. Mukhopadhyay and N. Rai, “Holographic Fermi surfaces in the six- dimensional (2, 0) theory,” *Phys. Rev. D* **96**, no. 2, 026005 (2017). doi:10.1103/PhysRevD.96.026005
- [29] S. Mukhopadhyay and N. Rai, “Holographic Fermi surface at finite temperature in six-dimensional (2, 0) theory,” *Phys. Rev. D* **96**, no. 6, 066001 (2017). doi:10.1103/PhysRevD.96.066001

- [30] N. Iqbal, H. Liu and M. Mezei, “Lectures on holographic non-Fermi liquids and quantum phase transitions,” [arXiv:1110.3814].
- [31] M. Vojta, Lattice symmetry breaking in cuprate superconductors: Stripes, nematics and superconductivity, *Adv. Phys.* 58 (2009) 699, arXiv:0901.3145 [cond-mat].
- [32] Shin Nakamura, Hirosi Ooguri, Chang-Soon Park, “Gravity Dual of Spatially Modulated Phase,” *Phys.Rev.D*81:044018,2010, arXiv:0911.0679 [hep-th]
- [33] Hirosi Ooguri, Chang-Soon Park, “Holographic End-Point of Spatially Modulated Phase Transition,” *Phys.Rev.D*82:126001,2010, arXiv:1007.3737
- [34] Aristomenis Donos and Jerome P. Gauntlett, “Holographic striped phases,” *JHEP* 1108 (2011) 140, arXiv:1106.2004
- [35] Aristomenis Donos, Jerome P. Gauntlett, “Holographic helical superconductors,” *JHEP* 1112 (2011) 091, arXiv:1109.3866
- [36] Aristomenis Donos, Jerome P. Gauntlett, “Black holes dual to helical current phases,” *Phys.Rev. D*86 (2012) 064010
- [37] Aristomenis Donos, “Striped phases from holography,” *JHEP* 1305 (2013) 059, arXiv:1303.7211 [hep-th]
- [38] Aristomenis Donos, J. P. Gauntlett, and C. Pantelidou, “Spatially modulated instabilities of magnetic black branes,” *JHEP* 01, 061 (2012), arXiv:1109.0471 [hep-th].
- [39] Sera Cremonini and Annamaria Sinkovics, “Spatially Modulated Instabilities of Geometries with Hyperscaling Violation,” *JHEP* 1401 (2014) 099
- [40] Sera Cremonini, “Spatially Modulated Instabilities for Scaling Solutions at Finite Charge Density, *Phys. Rev. D* 95, 026007 (2017), arXiv:1310.3279
- [41] Sera Cremonini, Li Li , Jie Ren, “Holographic Pair and Charge Density Waves,” *Phys.Rev. D*95 (2017) no.4, 041901, arXiv:1612.04385
- [42] Sera Cremonini, Li Li , Jie Ren, “Holographic Fermions in striped superconductors,” *JHEP* 1812 (2018) 080 , arXiv:1807.11730
- [43] Benjamin Withers, “Black branes dual to striped phases,” *Class.Quant.Grav.* 30 (2013) 155025, arXiv:1304.0129
- [44] Moshe Rozali, Darren Smyth, Evgeny Sorkin and Jared B Stang, “Striped order in AdS/CFT,” *Phys. Rev. D* 87, (2013) 126007 , arXiv:1304.3130
- [45] Benjamin Withers, “Holographic Checkerboards,” *JHEP* 1409 (2014) 102 , arXiv:1407.1085

- [46] Benjamin Withers, “The moduli space of striped black branes,” arXiv:1304.2011 [hep-th].
- [47] Andrea Amoretti, Daniel Are'an, Blaise Goute'raux and Daniele Musso, “Effective holographic theory of charge density waves,” Phys.Rev. D97 (2018) no.8, 086017 , arXiv:1711.06610; “DC resistivity of quantum critical, charge density wave states from gauge-gravity duality,” Phys.Rev.Lett. 120 (2018) no.17, 171603, arXiv:1712.07994
- [48] Aristomenis Donos, Jerome P. Gauntlett, “Holographic charge density waves,” Phys.Rev. D87 (2013) no.12, 126008
- [49] Blaise Goute'raux, Victoria L. Martin, “Spectral weight and spatially modulated instabilities in holographic superfluids,” JHEP 1705 (2017) 005, arXiv:1612.03466
- [50] Oren Bergman, Niko Jokela, Gilad Lifschytz and Matthew Lippart, “Striped instability of a holographic Fermi-like liquid,” JHEP, 10 (2011), 034, ArXiv: 1106.3883
- [51] N. Jokela, M. Jarvinen and M. Lippert, “A holographic quantum Hall model at integer filling”, JHEP **1105**, 101 (2011), doi:10.1007/JHEP05(2011)101, [arXiv:1101.3329 [hep-th]].
- [52] Niko Jokela, Matti Jarvinen and Mathew Lippart, “Fluctuations and instabilities of a holographic metal,” JHEP, 02 (2013),007, arXiv:1211.1381
- [53] Niko Jokela, Matti Jarvinen, Matthew Lippert, “Gravity dual of spin and charge density waves,” JHEP 1412 (2014) 083, arXiv:1408.1397 [hep-th]
- [54] Y. Liu, K. Schalm, Y. W. Sun and J. Zaanen, “Lattice potentials and fermions in holographic non Fermi-liquids: hybridizing local quantum criticality, JHEP 1210 (2012) 036 [arXiv:1205.5227].
- [55] Y. Ling, C. Niu, J. P. Wu, Z. Y. Xian and H. b. Zhang, Holographic fermionic liquid with lattices,” JHEP 1307 (2013) 045 [arXiv:1304.2128].
- [56] S. Cremonini, L. Li and J. Ren, “Holographic Fermions in Striped Phases,” JHEP **12**, 080 (2018) doi:10.1007/JHEP12(2018)080 [arXiv:1807.11730 [hep-th]].
- [57] N. Rai and S. Mukhopadhyay, “Holographic charge density wave from D2-D8,” JHEP **05**, 109 (2020) doi:10.1007/JHEP05(2020)109 [arXiv:1909.03458 [hep-th]].
- [58] J. P. Boyd, Chebyshev and Fourier spectral methods, 2nd edition, Dover, New York, 2001
- [59] N. Iqbal and H. Liu, “Real-time response in AdS/CFT with application to spinors,” Fortsch. Phys. **57**, 367 (2009) doi:10.1002/prop.200900057 [arXiv:0903.2596 [hep-th]].

- [60] S. Cremonini, L. Li and J. Ren, “Spectral Weight Suppression and Fermi Arc-like Features with Strong Holographic Lattices,” JHEP **09**, 014 (2019) doi:10.1007/JHEP09(2019)014 [arXiv:1906.02753 [hep-th]].
- [61] X. L. Lei, C. S. Ting and J. L. Birman, “Spectral function of the charge- density-wave (CDW) phonon in an anisotropic CDW superconductor”, Phys. Rev. B30, (1984), no. 11, 6387.